AAS 08-086

THE ORBITAL REGIME INDEX: A COMPREHENSIVE PARAMETER TO DETERMINE ORBITAL REGIONS AROUND MINOR BODIES

Carmine Buonagura* and Carmine Giordano† and Fabio Ferrari‡ and Francesco Topputo§

Understanding the characteristics and environmental conditions around minor celestial bodies is of paramount importance for gaining insights into the perturbations that can affect the orbit of a spacecraft when it is in their close proximity. Minor celestial bodies exhibit a wide range of physical properties, making it imperative for autonomous guidance, navigation, and control (GNC) algorithms to be robust in the face of the uncertainties associated with these celestial objects. Within the scope of this study, we aim to point out the relationships among the primary characteristics of minor bodies while establishing distinct orbital regimes based on their unique attributes such as shape, size, and density. By doing so, our research seeks to identify the specific conditions under which periodic orbits and active control strategies can be effectively employed in close proximity to these small celestial objects. This investigation holds significant implications for space exploration and mission planning, as it provides valuable insights into how to optimize spacecraft operations and navigate safely around minor bodies. Notably, our analysis can serve as a preliminary tool for mission analysts to assess the most promising GNC strategies based on mission requirements and the characteristics of the celestial bodies in question.

INTRODUCTION

Exploration of minor celestial bodies is increasingly attracting interest. Various space missions have targeted these objects due to the potential for significant scientific and engineering breakthroughs they offer.[1–3] Within this context, it becomes imperative to tackle the challenges inherent in operating in low-gravity, deep-space environments. A comprehensive understanding of the dynamics in the close proximity of these celestial objects becomes crucial for optimizing the scientific and technological yield of these missions. This becomes particularly relevant when employing cost-effective platforms like CubeSats, which operate with limited onboard resources and maneuvering capabilities. Therefore, thorough design and careful mission profile planning play a key role in maximizing the effectiveness of these missions. The environment surrounding a minor celestial body is characterized by a high degree of nonlinearity, resulting from its intrinsic complexity. Additionally, the abundance of uncertainties in its dynamical nature further amplifies it. Understanding this environment is of crucial importance, as it provides insights into the various perturbations that

*PhD Student, Department of Aerospace Science and Technology, Politecnico di Milano, Via La Masa 34, 20156, Milan, Italy.

†Post Doc, Department of Aerospace Science and Technology, Politecnico di Milano, Via La Masa 34, 20156, Milan, Italy.

‡Associate Professor, Department of Aerospace Science and Technology, Politecnico di Milano, Via La Masa 34, 20156, Milan, Italy.

§Full Professor, Department of Aerospace Science and Technology, Politecnico di Milano, Via La Masa 34, 20156, Milan, Italy.

can affect the trajectory of a spacecraft. These perturbations, arising from factors such as irregular gravitational fields and non-uniform mass distributions, require a thorough understanding to constructively exploit the nonlinear behavior. Comprehensive understanding of this environment is essential for developing effective GNC strategies, optimizing orbital maneuvers, and ensuring mission success.

Minor bodies exhibit diverse characteristics, including a wide range of shapes, sizes, compositions, and morphological features.[4] Shapes can vary from spherical to elongated, irregular, and bilobed, with sizes spanning from a few meters to thousands of kilometers.[5] Their structures range from rubble-pile,[6] characterized by the aggregation of boulders that are kept together by mutual gravity, to monolithic blocks, assumed for smaller and fast rotators. There are three different techniques to estimate size and shape of minor bodies, each offering a different degree of accuracy:[7]

- *Light curve analysis*: this method relies on observing the light curves of asteroids and comets over extended periods, providing a rough approximation of their shape. However, finer details like craters and boulders may not be accurately represented.
- *Radar range–doppler imaging*: this method exploits on-ground radio antenna. It enables a more accurate estimation of shape and spin, achieving resolutions on the order of several tens of meters.
- *High-resolution imagery*: this technique exploits the combination of visual imagery taken at different viewing geometries and phase angles. This method is employed during rendezvous and flyby missions, offering the highest resolutions in the order of few meters. Flyby targets often cannot achieve global shape reconstruction due to the limited observation time and constrained geometry. Another instrument that surpasses the resolutions achieved by cameras is the use of LIDAR.

The diversity in composition among minor celestial bodies is also notable, encompassing both uniform and heterogeneous structures composed of various elements. This diversity results in a wide range of densities across these celestial objects. Asteroids, in particular, can be broadly classified based on their composition into three main types.[8] C-type (carbonaceous) asteroids exhibit a visually dark appearance and are primarily composed carbon, making them the most common among the three types. S-type asteroids consist predominantly of silicate materials and nickel-iron. On the other hand, M-type asteroids are primarily composed of metals, with nickel and iron being the most prevalent elements.

Understanding all these characteristics is crucial for designing guidance, navigation, and control algorithms in proximity to minor bodies, as the dynamical environment can significantly vary based on the considered body properties, which are often uncertain.
Past missions, such as the NASA's Double Asteroid Redirection Test (DART),[9] highlight the uncertainties surrounding the main physical parameters of these bodies. For instance, Dimorphos, the primary asteroid of the (65803) Didymos binary system, was initially expected to be a diamond-shaped asteroid, with an equatorial bulge and flattened poles.[10] However, DART's approach revealed its strongly oblate shape.[11]
To enable autonomy and reduce the need for continuous ground intervention, GNC algorithms must be robust in the face of uncertainties in the dynamical and morphological environments of minor bodies. The aim of this work is to investigate the existence of general orbital regions in proximity

to minor bodies, facilitating safe approaches, characterization, and a gradual reduction in orbital altitude leading to the possibility of landing on these celestial bodies.

Various studies have explored the dynamical field in the vicinity of minor bodies, taking into consideration the actual density and size values of the specific body under examination.[12–19] However, some researchers have opted to consider multiple or modeled shapes of minor bodies to evaluate the resilience of algorithms.[20–22] Notably, none of these prior works have holistically considered both the shapes and physical properties of minor bodies. This study seeks to address this gap by comprehensively analyzing the dynamical environment of a diverse range of minor bodies, accounting for variations in shapes, sizes, and densities. The approach involves categorizing the dynamical environment into distinct orbital regions based on the acceleration field in close proximity to the celestial body and highlighting their relationship by introducing the Orbital Regime Index ($\mathcal{ORI}$). This novel perspective aims to provide a more integrated understanding of the challenges posed by minor bodies and enhance the robustness of algorithms in navigating these complex and varied environments.

The paper is structured as follows. The initial part of the study covers the selection of minor bodies for analysis, outlines the modeled dynamical environment, and provides definitions for the orbital regions in the proximity of minor bodies. Following this, the primary findings of the study are presented. Specifically, a method for estimating orbital regions based on the shape and size of a generic body is introduced, and various orbital regimes are discussed. The study concludes with a discussion of some final considerations.

METHODOLOGY

In this section, we discuss the methodology for the selection of representative bodies, the modeling of the dynamical environment, and the definition of gravity regions. Additionally, we explore significant indices to quantitatively describe the environment around minor bodies.

Bodies Selection

Minor bodies exhibit a variety of sizes, shapes, compositions, and morphological features. Due to the vast array of characteristics they present, it is necessary to select representative models to conduct a comprehensive analysis that can be generalized to any encountered body. Shape models of asteroids and comets are continuously estimated, with a total of 4476 minor bodies available[*†‡]. Among these models, 4443 were obtained through light curve analysis, 8 through close approach imagery, and 21 through radar observations. Additionally, there are 4 available comet models.
For each body, orbital and physical parameters have been downloaded[§]. However, several of them lack assigned properties. While parameters such as absolute magnitude and rotational period are be easily assessed through light curve analysis, others, including albedo, size, and density, are not readily available and must be estimated. The reasoning followed for estimating these parameters is outlined below.

[*] `https://astro.troja.mff.cuni.cz/projects/damit/asteroids/browse`, Last access: January 4, 2024

[†] `https://sbn.psi.edu/pds/shape-models/`, Last access: January 4, 2024

[‡] `https://3d-asteroids.space/`, Last access: January 4, 2024

[§] `https://ssd.jpl.nasa.gov/`, Last access: January 4, 2024

To address the limited range of values that albedo can assume,[5] a rough estimation has been performed, considering a folded normal distribution with mean $\bar{\mu} = 0.130$ and standard deviation $\sigma = 0.153$.

When size information is unavailable, it is computed using albedo and the absolute magnitude from light curve observations. The equation to compute the equivalent asteroid diameter d is:[23]

$$d = 10^{3.1235 - \frac{1}{2}\log_{10} A - 0.2H} \tag{1}$$

where A is the albedo, and H represents the absolute magnitude.

Regarding the density ρ, considered uniform in this work, it is estimated based on the spectral type of the asteroid, utilizing mean and standard deviation values available for each asteroid type[24] and a folded normal distribution. If the type is not known a priori, general mean and standard deviation values are considered ($\bar{\mu} = 2.78\ g/cm^3$, $\sigma = 2.59\ g/cm^3$). Once size and density are available, mass, and consequently, the gravitational constant μ, can be computed.

Shape parameters, namely elongation el, flatness fl, and irregularity ir, are defined from the body shape model. To estimate elongation and flatness, a linear least-square problem is solved to fit an ellipsoid to the point cloud[25] represented by the vertices of the minor body mesh. Once the semi-axes of the ellipsoid $(\bar{a}, \bar{b}, \bar{c})$ are computed, with $\bar{a} \geq \bar{b} \geq \bar{c}$, the elongation and flatness can be estimated as follows:

$$el = 1 - \frac{\bar{b}}{\bar{a}} \tag{2}$$

$$fl = 1 - \frac{\bar{c}}{\bar{b}} \tag{3}$$

These metrics range from 0 (perfectly spherical surface), to 1 (asymptotic value for extremely elongated and flat body, respectively).
Regarding the irregularity, a metric is proposed to measure quantitatively the irregularity of the global shape of the body:

$$ir = 1 - \frac{S_e}{S} \tag{4}$$

where S is the body surface area, and S_e is the surface area of the Dynamically Equivalent Equal Volume Ellipsoid (DEEVE), having the same moments of inertia and volume of the examined minor body. The ir provides a measure of the irregularity of the body, with $S > S_e$ for any real, non-perfectly spherical object, ranging from 0 (perfectly spherical surface), to 1 (asymptotic value for extremely irregular body).

In Figure 1, a comprehensive plot with all the analyzed bodies along with the combination of significant parameters, namely equivalent diameter d, rotational period T, gravitational constant μ, elongation el, flatness fl, and irregularity ir, is shown. There is no particular trend that arises from this analysis, but it is evident that the light curve analysis is unreliable since the shapes obtained with radar and images do not always align with the light curve cluster of points. For this reason, bodies considered for further analysis are selected from the radar, comets, and images clusters. In particular, the selected bodies are those with the maximum and minimum combination of el, fl, and ir. Their selection has been done by computing all the points on the Pareto fronts, linearly interpolating them, and choosing the point with the maximum distance from the interpolating line. From this approach, 8 different bodies are chosen, as shown in Figure 2. These 8 bodies, along with 4 others, including the regularly shaped asteroid (4) Vesta, an ideal unit sphere, an oblate sphere

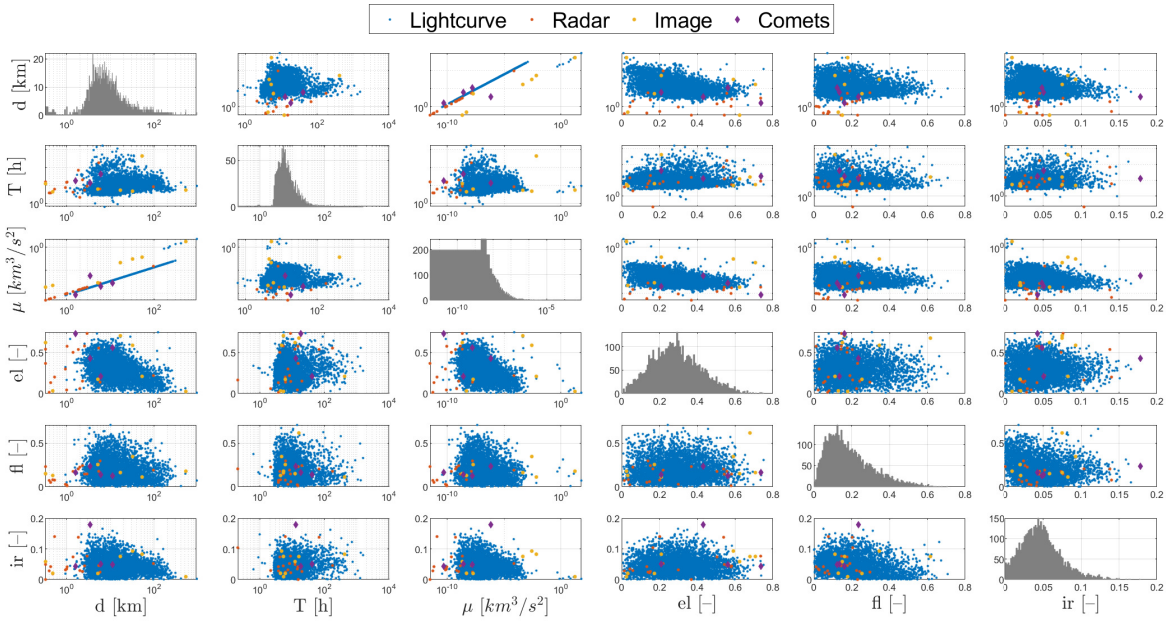

Figure 1 Minor bodies data analysis

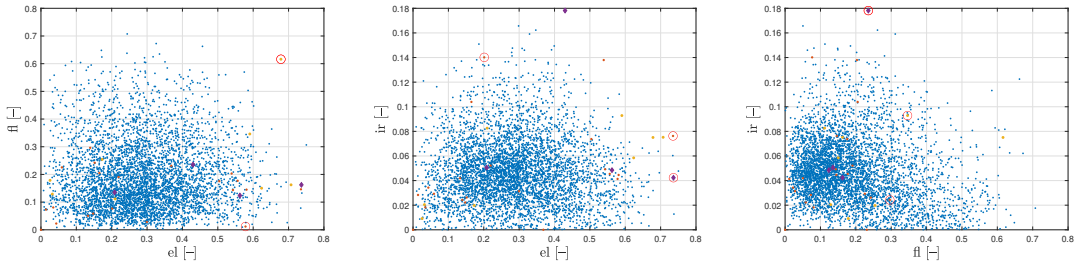

(a) (b) (c)

Figure 2 Selection of representative minor bodies circled in red

(Ellipsoid 1), and an ideal ellipsoid (Ellipsoid 2) with axes equal to $(1, 1, 0.5)$ and $(1, 0.5, 0.5)$ respectively, are considered for further analysis. The selected bodies and their shape metrics are listed in Table 1.

Dynamical Environment

In this section, the modeling of the dynamical environment near a general minor body is discussed and the equations that drive the dynamics of a CubeSat in its proximity are formalized.
Some assumptions have been made in order to simplify the model. The generic minor body under investigation is considered to be part of the Main Belt, with arbitrarily chosen orbital parameters reported in Table 2. Furthermore, the analyses are conducted at the time instant when the body is at its position along the orbit closest to the Sun to maximize its influence. The influence of Jupiter is

Table 1 Representative minor bodies

ID	Body name	el [−]	fl [−]	ir [−]
MB01	Sphere	0	0	0
MB02	Ellipsoid 1	0	0.5	0
MB03	Ellipsoid 2	0.5	0	0
MB04	(4) Vesta	0.03	0.18	0.01
MB05	(243) Ida	0.59	0.35	0.10
MB06	(1580) Betulia	0.14	0.30	0.02
MB07	(2063) Bacchus	0.58	0.01	0.04
MB08	(6489) Golevka	0.20	0.08	0.14
MB09	(8567) 1996 HW1	0.74	0.15	0.08
MB10	(486958) Arrokoth	0.68	0.62	0.08
MB11	(1000012) 67P/Churyumov-Gerasimenko	0.43	0.24	0.18
MB12	(1000041) 103P/Hartley 2	0.74	0.16	0.04

Table 2 Generic main belt asteroid orbital parameters

SMA $[AU]$	e [−]	i [deg]	Ω [deg]	ω [deg]
2.7	0.15	11	170	290

also considered. The bodies selected vary in sizes and densities, in order to span all possible minor body conditions in terms of physical properties and to conduct a significant comparison among the different shapes. Specifically, 7 different sizes s in terms of maximum distance from the center of mass, and 20 different densities ρ are taken from Figure 1 and reported in Table 3.

Table 3 Minor body sizes and densities considered.

$s\ [km]$	$(0.25, 0.5, 1, 2.5, 5, 50, 500)$
$\rho\ [g/cm^3]$	$[1.5, 11]$

The dynamic of the CubeSat is driven by four main accelerations: the gravity of the main celestial body $\mathbf{a_b}$, the third-body effect of the Sun $\mathbf{a_{3b_S}}$ and of the planet $\mathbf{a_{3b_P}}$, and the Solar Radiation Pressure (SRP) $\mathbf{a_{SRP}}$. All these quantities are expressed in a body fixed reference frame with axes aligned with the principal inertia moments of the selected shape. More details on the importance of each contribution are provided in the following. In their most general form, the equations of motion for a point mass in the proximity of a minor body read:

$$\ddot{\mathbf{r}} = \mathbf{a_b} + \mathbf{a_{3b_S}} + \mathbf{a_{3b_P}} + \mathbf{a_{SRP}} \tag{5}$$

The acceleration $\mathbf{a_b}$ is due to the central body specified with the Mascon model.[7,26–28] Specifically, the body is assumed to have a constant density and is divided into N equal mass tetrahedra, where N is the number of faces of the polyhedral model, such that the total mass of the body $m_b = \sum_{i=1}^{N} m_i$. This approximation is considered sufficient for the purposes of this work. The central body gravity

field is then computed as:

$$\mathbf{a_b} = -\sum_{i=1}^{N} \frac{\mu_i}{r_i^3}\mathbf{r_i} \tag{6}$$

where $\mathbf{r_i}$ is the position of the particle with respect to the geometric center of the considered tetrahedron and μ_i is its gravitational constant.

The third-body effect is the perturbative acceleration of an object different from the central body, and can be written as:

$$\mathbf{a_{3b}} = (\mu_{3b} + \mu_b)\frac{\mathbf{r_{b-3b}}}{r_{b-3b}^3} - \mu_{3b}\frac{\mathbf{r_{P-3b}}}{r_{P-3b}^3} \tag{7}$$

where $\mu_{3b} = Gm_{3b}$ and $\mu_b = Gm_b$ are the gravitational constants of the third body (the Sun or Jupiter) and the minor body, respectively, $\mathbf{r_{b-3b}}$ and $\mathbf{r_{P-3b}}$ are the position vectors of the minor body center of mass and the field point with respect to the third body considered, in the body fixed reference frame.

The last contribution of Eq. 5 is due to SRP that pushes the CubeSat away from the Sun. This contribution is computed using an SRP cannonball model:[29]

$$\mathbf{a_{SRP}} = \frac{P_0}{c}\left(\frac{D_{AU}}{r_{P-S}}\right)^2 \frac{C_r A_{SC}}{m_{SC}}\hat{\mathbf{r}}_{\mathbf{P-S}} \tag{8}$$

where P_0 ($1367\ W/m^2$) is the solar flux at 1 AU, c is the speed of light ($2.998 \times 10^8\ m/s$), D_{AU} is the Sun-–Earth distance ($1AU = 1.495 \times 10^{11}\ m$), C_r is the reflectivity coefficient of the CubeSat, A_{SC} is its equivalent surface area, and m_{SC} is its mass. The CubeSat is assumed to be a 6U, whose properties are listed in Table 4.

Table 4 Properties of the selected CubeSat

Format $[-]$	$m_{SC}\ [kg]$	$A_{SC}\ [m^2]$	$C_r\ [-]$
6U	12	0.51	1.23

Gravity Field Regions and Indices Definition

The uncertain and irregular shape of minor bodies strongly influences the shape of the gravity field. This study aims to demonstrate that the gravity field around an irregularly shaped object always evolves following the same behavior. Specifically, the iso-gravity surfaces, referred as iso-surfaces for simplicity, are similar to the body shape in its close proximity up to the distance at which they degenerate into ellipsoids. The portion of space from the body surface to the first iso-ellipsoid will be named irregular region. Once the gravity field becomes ellipsodial, its shape continues changing into increasing size ellipsoids up to the distance at which they becomes spherical. This is the ellipsoidal region, and it is bounded from the first iso-ellipsoid to the first iso-sphere. In this portion of space, the shape and morphological features of the body are no longer important, and the gravity field can be assumed to be the same as that of an ideal ellipsoid. By moving further away from this point, the gravity field results in being spherical, and consequently, gravity can be modelled by the simple point mass model. Another important region to define is the one where the body gravity field is dominant with respect to external perturbations (third body and SRP).

This region is strongly influenced by the size and density of the main body and is named Gravity Over Perturbations (GOP) region. In this work, the upper bound shape of the region has been defined when the body gravity field value is 90% higher than the accelerations due to the external perturbations, while the lower bound surface is the body surface itself. A schematic representation of the gravity regions is reported in Figure 3. Only the first iso-sphere of the spherical region is represented for simplicity. Since these regions strongly depend on the shape, size, and density

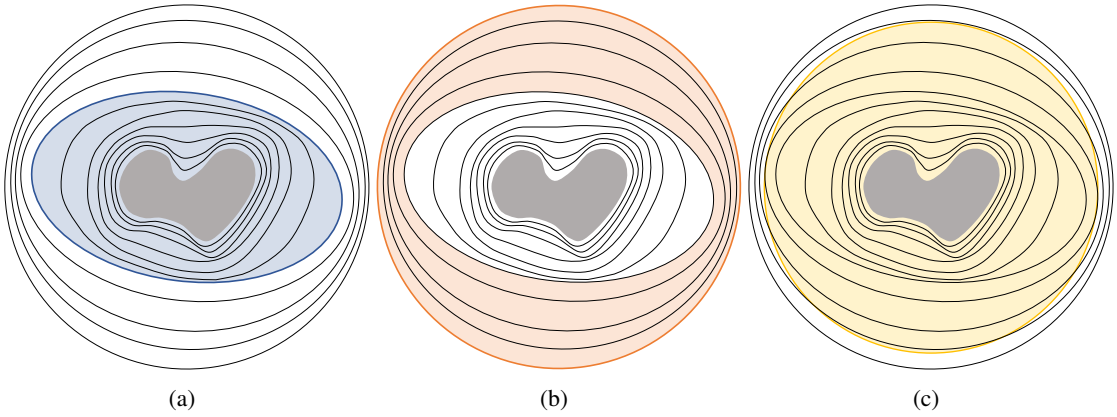

Figure 3 Definition of gravity regions around minor bodies. (a) Irregular, (b) ellipsoidal, and (c) GOP regions.

of the considered body, a robust algorithm to find the bounding surfaces of each region has been designed. Particularly, the iso-ellipsoid and iso-sphere have been computed solving a nested zero-finding approach.

Within each function evaluation of the outer zero-finding procedure, which is designed to identify an ellipsoidal or spherical-shaped surface, an additional zero-finding problem is addressed to determine the iso-gravity surfaces surrounding the minor body. The primary outcome is the computation of the minimum size ellipsoidal or spherical iso-gravity surface. The zero-finding procedures are described in the remainder of the section.

From the Brillouin sphere[30] of the selected body, 100 uniformly distributed points P are sampled. This sphere is the lower bound considered for the iso-surfaces as the gravity field inside it is by definition irregular. To find the minimum iso-gravity surface lying completely outside the Brillouin sphere, the minimum acceleration value among these points is considered as the lower bound for the outer zero-finding problem. The upper bound acceleration has been selected equal to its value at an arbitrary distance equal to 50 times the maximum dimension of the body, so that a spherical iso-surface is got.

The first condition, named *iso-gravity surface*, to be satisfied is that all the points lie on an iso-gravity surface, meaning that all the points have the same gravity value. To find this surface, each point is multiplied by a value x_i that goes from 1 to an arbitrarily high value to find the amount of displacement needed to get a gravity that is equal to a certain prescribed value a_0.

$$f(x_i) = a_b(x_i) - a_0 \tag{9}$$

The locus of the obtained points forms an iso-surface that is likely to have an irregular shape. To solve the problem, it is required to find the acceleration for which the iso-surface assumes a regular

shape, such that the one of a sphere or an ellipsoid. For this reason, the outer loop solves for the prescribed acceleration a_0.
Indeed, the second condition to be satisfied, named *conical surface*, must check that the computed iso-surface is an ellipsoid or a sphere. In the following, we will only discuss about the ellipsoid, but the procedure is exactly equivalent for the spherical case.
The iso-surface computed with the described approach is fitted by an ellipsoid, and the gravity value of more than 2000 points a_{P_e} lying on it are computed. The gravity field is considered ellipsoidal if the relative percentual error e among the points P_e is lower than 1%.

$$e = \frac{\max(a_{P_e}) - \min(a_{P_e})}{\text{mean}(a_{P_e})} < 0.01 \tag{10}$$

If the *iso-gravity* and *conical surface* conditions are both satisfied, the ellipsoidal iso-surface is found. The exact same procedure applies for the iso-sphere.
Regarding the GOP region, the inner loop is sufficient to solve for the GOP surface. Specifically, the displacements x_i are calculated to identify points where the gravitational influence of the central body exceeds a certain percentage relative to the perturbations. The nonlinear equation being solved is expressed as follows:

$$g(x_i) = \frac{a_b(x_i) - a_p(x_i)}{a_b(x_i)} 100 - 90 \tag{11}$$

where a_p is the acceleration due to the perturbative effects, namely third body and SRP.

Once these relevant regions are defined, parameters to describe their relative size are required. The orbital regime index has been conceptualized considering all the discussed orbital regions. It gives an indication of the relative dimension of the orbital regions, and thus the best guidance strategy to use based on the body at hand. It is made up of 3 different parameters, which are the field irregularity ($\mathcal{FI}$), ellipsicity ($\mathcal{FE}$), and quiescence ($\mathcal{FQ}$). The $\mathcal{ORI}$ can be computed with the following:

$$\mathcal{ORI} = [\mathcal{FI}, \mathcal{FE}, \mathcal{FQ}] = \left[\left(\frac{V_e}{V_b} \right)^{\frac{1}{3}}, \left(\frac{V_s}{V_e} \right)^{\frac{1}{3}}, \left(\frac{V_{GOP}}{V_s} \right)^{\frac{1}{3}} \right] \tag{12}$$

where V_s, V_e, and V_{GOP} represent the volume of the iso-sphere, iso-ellipsoid, and GOP, respectively. The values assumed by these parameters were reported in the range $[0, 1]$, for this reason, their minimum and maximum value were computed for each of the considered bodies. In our current knowledge, they are the worst case shapes in terms of elongation, flatness, and irregularity, but as most strange shapes can exist in nature, the maxima are increased by an order of magnitude. A logarithmic interpolation has been made to obtain a value that is equal to 0 when the parameters assume their minimum value, while a value of 1 when the maximum is reached. When they are 0, it means that the gravity field is not influenced by the shape of the body, is spherical, and is not affected by perturbations, while when they assume a value of 1, the field is highly irregular, elliptical, and perturbed.

RESULTS

This section presents the primary findings of this study. Overall orbital regions trend are derived from the analyzed values of densities and sizes, and an estimation method of these regions is outlined based on body shape parameters. Different orbital scenarios are presented for each selected body under the conditions of minimum size and density. Finally, the variation in $\mathcal{ORI}$ is shown in response to changes in the physical parameters of the bodies.

Variable Size and Density

The identified orbital regions strongly depend on the shape, size, and density of the main body. In this section, trends independent of shape are firstly described, and subsequently, an estimation technique for the iso-surfaces based on the shape of the body is discussed.
Specifically, the orbital regions have been computed for each body for each size–density combination, yielding clear trends illustrated in Figure 4. Notably, a linear correlation emerges, revealing that the size of the regions scales proportionally with the size of the body, regardless of its density. Upon increasing the size of the central body, both the iso-ellipsoid and iso-sphere undergo proportinal inflation. Conversely, when transitioning towards higher densities while maintaining a constant size, the surfaces remain unaltered, but there is an increase in acceleration values. Turning to the GOP region, its dimensions are predictably influenced by the mass of the body, leading to a stronger gravitational attraction. Indeed, the GOP region attains its maximum size at the top right of Figure 4(b). The values associated with the iso-ellipsoid, iso-sphere, and GOP regions are qualitatively depicted as ranging from 0 to 1. This representation is chosen to underscore the overall trend, as distinct values are obtained for each shape.

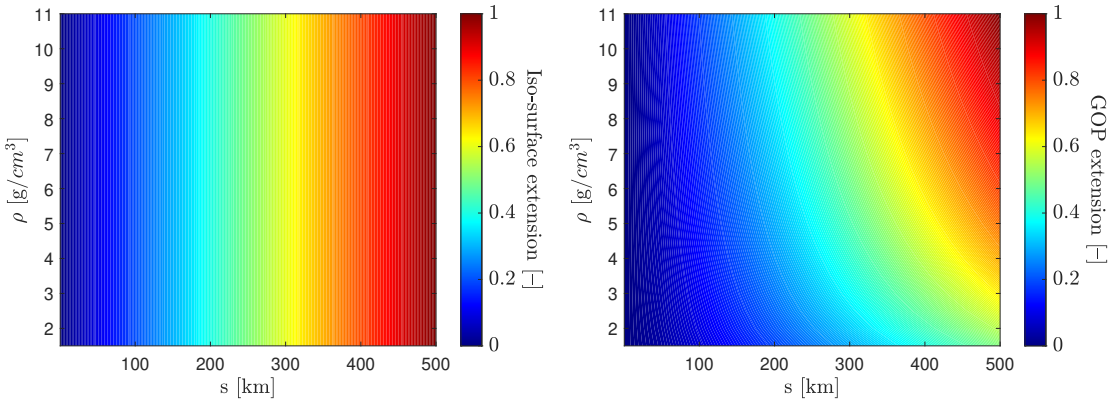

Figure 4 Orbital regions trends as a function of size and density. (a) Iso-ellipsoid, iso-sphere, and (b) GOP region trend

This analysis reveals that the iso-surfaces are independent of the density value. Therefore, it is possible to estimate their size solely by knowing the size and shape of the considered body. The methodology employed involves determining the multiplicative factor $\int_\rho$ required to obtain the iso-surfaces of both the ellipsoid and sphere based on the size of the celestial body. For each selected body, this factor has been computed, offering valuable insights. Clearly, the multiplicative factor for the iso-ellipsoid consistently proves to be either lower or equal to that of the iso-sphere. Figure 5 presents these multiplicative factors for the selected celestial bodies, highlighting their variations. This approach unveils a potential tool for estimating the size of orbital regions for a given minor body with a known shape. By identifying the body with the most similar shape parameters, one can utilize the corresponding multiplicative factor to make a preliminary estimation of the orbital regions for the generic body. This methodology allows rapid assessment of the irregularity of the gravity field in proximity to the body. If the multiplicative factor of the two iso-surfaces coincide and deviates from 1, it reports a highly irregular acceleration field, necessitating the design of active

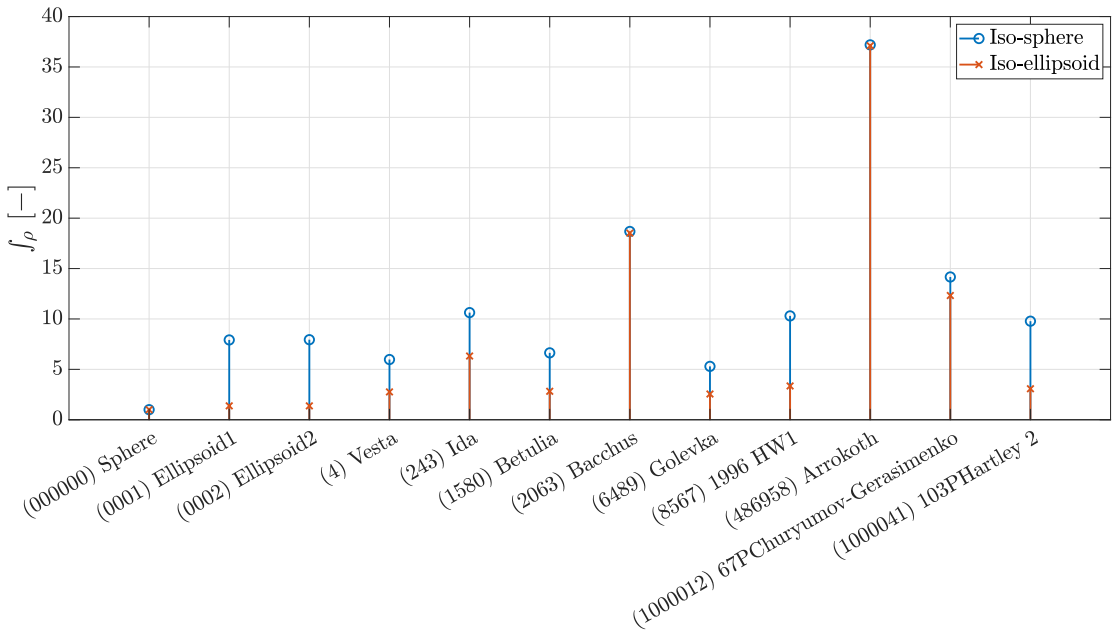

Figure 5 Estimation of orbital regions as a function of the shape of the body

control strategies to manage the irregularities effectively. Thanks to this analysis, we can conclude that two of the three parameters composing the $\mathcal{ORI}$, namely $\mathcal{FI}$ and $\mathcal{FE}$, do not depend on the size and density of the body but solely on its shape.

Orbital Regimes

The size of the orbital regions exhibits a strongly dependence on the specific shape of the body under consideration. The only condition for which the three bounding surfaces assume a comparable size arises when the density of the body equals $1.5\ g/cm^3$ and its size stands at $0.25\ km$. Figure 6 serves as a visual representation of the different conditions that emerge based on the body shape. This figure emphasizes the complex relationship between a body geometric attributes and its gravitational characteristics, revealing that a specific combination of density and diameter can lead to orbital regions of different sizes depending on the shape of the body. From this analysis, four different orbital conditions arise. Three specific cases are identified when the $\mathcal{FE}$ is 0, where the iso-ellipsoid aligns with the iso-sphere, as illustrated in Figures 6(a), 6(g), and 6(j). This scenario occurs in cases of a perfectly spherical body ($\mathcal{FI} = 0$) or one exhibiting extreme elongation and irregularity ($\mathcal{FI} >> 0$). The first scenario represents the ideal condition where the body can be treated effectively as a point mass, allowing for the exploitation of periodic orbits. However, for celestial bodies like (2063) Bacchus and (486958) Arrokoth, with this specific size–density combination, orbital dynamics become highly challenging due to the irregular gravity field in close proximity and the dominance of perturbations.(486958) Arrokoth, in particular, presents additional complexities because of its peculiar shape, resulting from the union of a binary system into a single body. Another scenario, evident in Figures 6(b), 6(d), 6(f), and 6(h), occurs when the iso-ellipsoid is close to the body ($\mathcal{FI} << 1$), and both iso-surfaces are smaller than the GOP region. While the

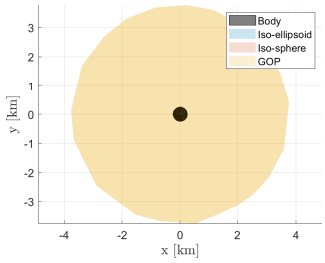

(a) MB01. $\mathcal{ORI} = [0, 0, 0.46]$

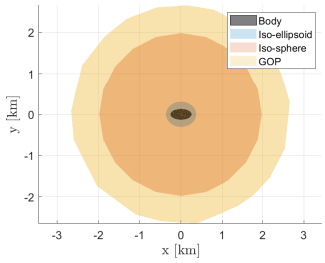

(b) MB02. $\mathcal{ORI} = [0.08, 0.43, 0.23]$

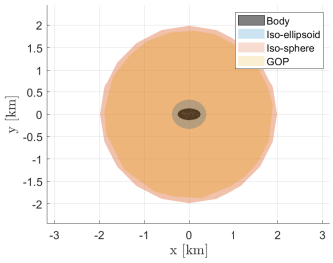

(c) MB03. $\mathcal{ORI} = [0.12, 0.43, 0.20]$

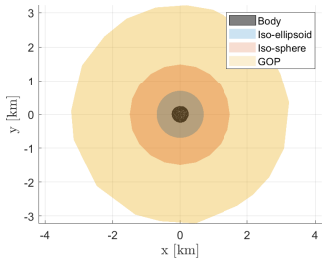

(d) MB04. $\mathcal{ORI} = [0.17, 0.19, 0.28]$

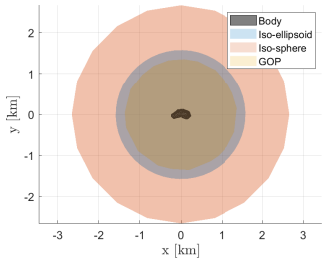

(e) MB05. $\mathcal{ORI} = [0.37, 0.13, 0.14]$

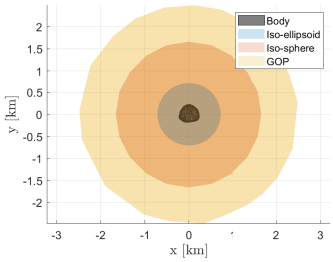

(f) MB06. $\mathcal{ORI} = [0.19, 0.21, 0.24]$

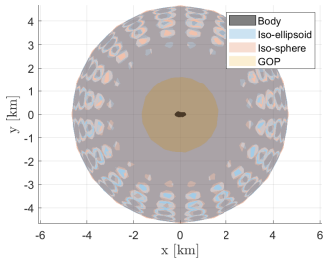

(g) MB07. $\mathcal{ORI} = [0.52, 0, 0.11]$

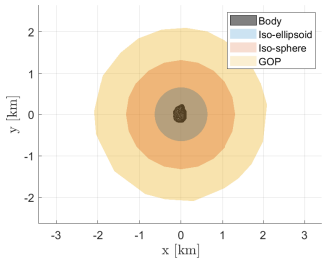

(h) MB08. $\mathcal{ORI} = [0.19, 0.18, 0.25]$

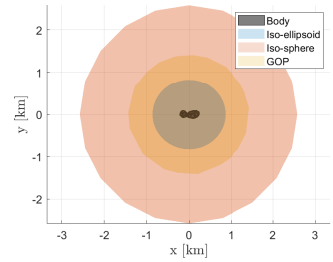

(i) MB09. $\mathcal{ORI} = [0.28, 0.28, 0.15]$

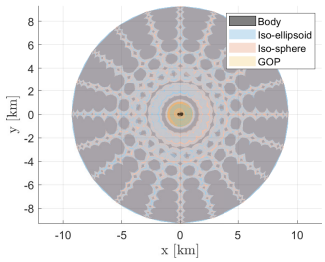

(j) MB10. $\mathcal{ORI} = [0.66, 0, 0]$

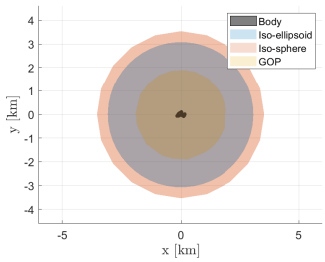

(k) MB11. $\mathcal{ORI} = [0.45, 0.03, 0.15]$

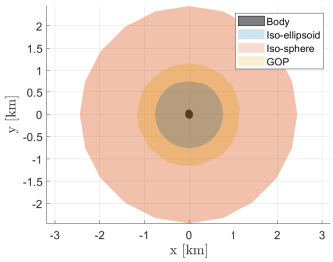

(l) MB12. $\mathcal{ORI} = [0.27, 0.29, 0.13]$

Figure 6 Orbital scenarios depending on the shape of the body

ellipsoidal and spherical regions prove useful for orbital purposes, the risk of drifting outside the GOP is notable, leading to a predominant influence of the SRP. This scenario happens for regularly, not elongated bodies whose $\mathcal{FQ}$ ranges from 0.23 to 0.28. Figures 6(e) and 6(k) depict a condition where the GOP region is enclosed within both iso-surfaces, demanding the counteraction of the SRP or highly risky close-proximity maneuvers accepting the highly irregular gravity field. Lastly,

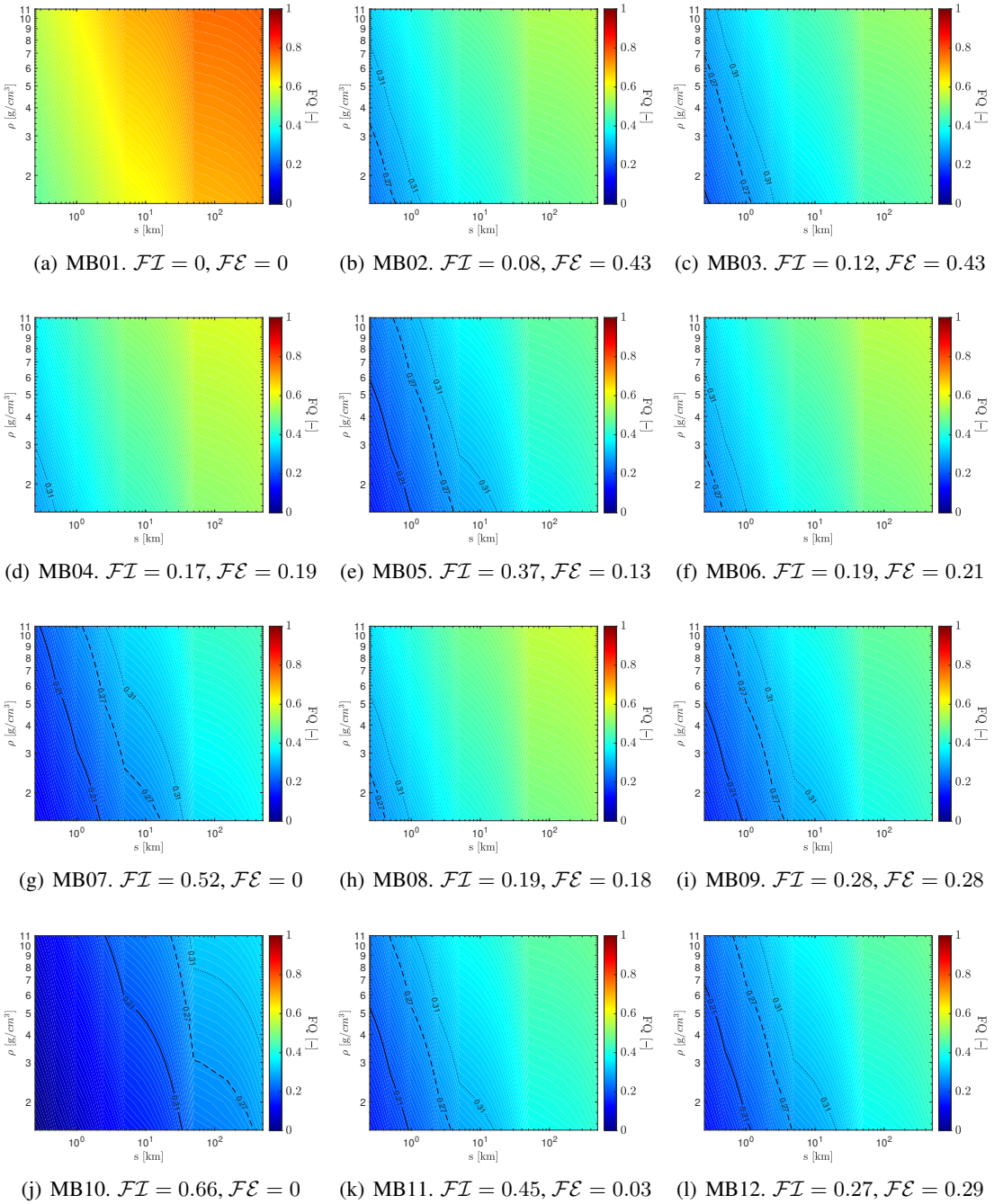

(a) MB01. $\mathcal{FI} = 0$, $\mathcal{FE} = 0$ (b) MB02. $\mathcal{FI} = 0.08$, $\mathcal{FE} = 0.43$ (c) MB03. $\mathcal{FI} = 0.12$, $\mathcal{FE} = 0.43$

(d) MB04. $\mathcal{FI} = 0.17$, $\mathcal{FE} = 0.19$ (e) MB05. $\mathcal{FI} = 0.37$, $\mathcal{FE} = 0.13$ (f) MB06. $\mathcal{FI} = 0.19$, $\mathcal{FE} = 0.21$

(g) MB07. $\mathcal{FI} = 0.52$, $\mathcal{FE} = 0$ (h) MB08. $\mathcal{FI} = 0.19$, $\mathcal{FE} = 0.18$ (i) MB09. $\mathcal{FI} = 0.28$, $\mathcal{FE} = 0.28$

(j) MB10. $\mathcal{FI} = 0.66$, $\mathcal{FE} = 0$ (k) MB11. $\mathcal{FI} = 0.45$, $\mathcal{FE} = 0.03$ (l) MB12. $\mathcal{FI} = 0.27$, $\mathcal{FE} = 0.29$

Figure 7 $\mathcal{FQ}$ parameter as a function of size and density of the selected bodies

in Figures 6(c), 6(i), and 6(l), the GOP region is between the iso-ellipsoid and the iso-sphere, defining a small elliptical region where the SRP is not predominant. The most favorable scenario occurs when the iso-sphere is positioned close to the body surface, along with a large GOP region. This configuration provides an extensive region favorable to accurate body characterization, facilitating subsequent transitions towards the ellipsoidal region, and eventually to the irregular one. While $\mathcal{FI}$ and $\mathcal{FE}$ remain constant regardless of size and density, $\mathcal{FQ}$ shows variations with these parameters. Consequently, Figure 7 illustrates the values of $\mathcal{FQ}$ for each size–density combination, leading to distinct conclusions.

The logarithmic normalization applied to $\mathcal{FQ}$ allows us to state that the GOP and iso-sphere overlap (V_{GOP} equals V_S) when the parameter is set to 0.21. This figure reveals that for bodies larger than $2.5\ km$, the GOP always lies outside the iso-sphere, regardless of the density of the body. It is noteworthy that for peculiar bodies like (486958) Arrokoth, a size greater than $35\ km$ is required due to its unique nature, which makes (486958) Arrokoth excluded from further analyses.
To achieve a GOP region with double or triple the volume of the iso-sphere, the $\mathcal{FQ}$ values must surpass thresholds of 0.27 and 0.31, respectively.
For bodies larger than $20\ km$, the GOP is always at least double the size of the iso-sphere, resulting in the presence of a significant spherical orbital region. When excluding the asteroid (2063) Bacchus, this size threshold significantly reduces to $3\ km$. Furthermore, for those seeking a larger spherical region where the GOP volume is three times that of the iso-sphere, bodies must have a size exceeding $30\ km$ (or $20\ km$ without considering (2063) Bacchus).

A peculiar orbital case is shown in Figure 8, in which the three orbital bounding surfaces coincide. This scenario happens when the size of (486958) Arrokoth is equal to $5\ km$ and its density equals $5.5\ g/cm^3$.
For asteroid (243) Ida and comet 67P/Churyumov-Gerasimenko all the possible orbital scenarios previously described can happen depending on the shape and density of the body. These scenarios are shown in Figure 9.

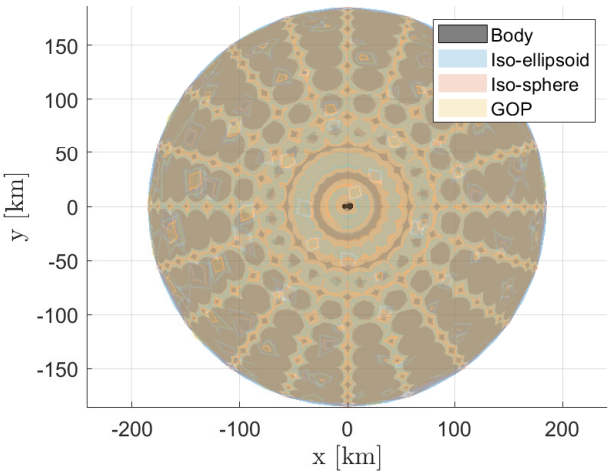

Figure 8 Asteroid (486958) Arrokoth with overlapping bounding surfaces

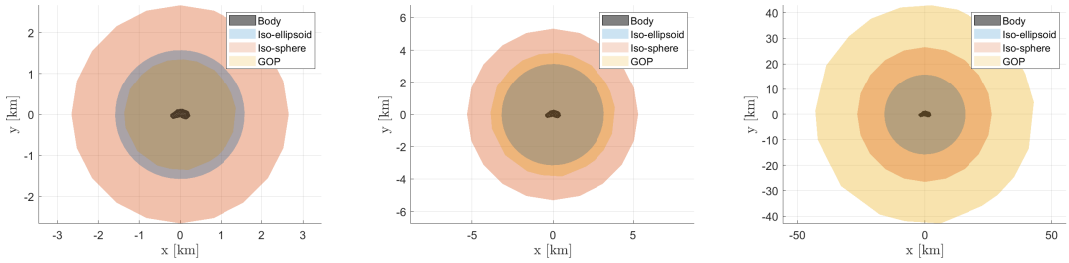

(a) (b) (c)

Figure 9 Asteroid (243) Ida orbital scenarios. GOP (a) inside, (b) between, and (c) outside iso-surfaces

CONCLUSION

Understanding the dynamic and morphological characteristics of minor bodies, including their diverse shapes, sizes, compositions, and gravitational fields, is essential for designing effective guidance, navigation, and control algorithms. This study comprehensively analyzes the dynamical environment of a diverse range of minor bodies, considering variations in shapes, sizes, and densities. The findings reveal distinct orbital regions influenced by these parameters, providing valuable insights for safe operations in close proximity to these celestial bodies. A comprehensive index is defined to provide a quantitative measure of the relative size of the various regions. The methodology developed, including the estimation of orbital regions based on body shape parameters, offers a rapid assessment tool for the irregularity of gravity fields in proximity to a minor body, along with indications of the most favorable orbital regions based on the body size.

REFERENCES

[1] M. Quadrelli, L. Wood, J. Riedel, M. McHenry, M. Aung, L. Cangahuala, R. Volpe, P. Beauchamp, and J. Cutts, "Guidance, navigation, and control technology assessment for future planetary science missions," *Journal of Guidance, Control, and Dynamics*, Vol. 38, No. 7, 2015, pp. 1165–1186.

[2] E. Asphaug, "Growth and evolution of asteroids," *Annual Review of Earth and Planetary Sciences*, Vol. 37, 2009, pp. 413–448.

[3] K. Zacny, P. Chu, J. Craft, M. Cohen, W. James, and B. Hilscher, "Asteroid mining," *AIAA SPACE 2013 Conference and Exposition*, 2013.

[4] W. F. Bottke Jr, A. Cellino, P. Paolicchi, and R. P. Binzel, "An overview of the asteroids: The asteroids III perspective," *Asteroids III*, Vol. 1, 2002, pp. 3–15.

[5] D. Morrison, "Asteroid sizes and albedos," *Icarus*, Vol. 31, No. 2, 1977, pp. 185–220.

[6] K. J. Walsh, "Rubble Pile Asteroids," *Annual Review of Astronomy and Astrophysics*, Vol. 56, No. 1, 2018, pp. 593–624.

[7] D. J. Scheeres, *Orbital motion in strongly perturbed environments: applications to asteroid, comet and planetary satellite orbiters*. Springer, 2016.

[8] D. J. Tholen and M. A. Barucci, "Asteroid taxonomy.," *Asteroids II*, 1989, pp. 298–315.

[9] A. F. Cheng, A. S. Rivkin, P. Michel, J. Atchison, O. Barnouin, L. Benner, N. L. Chabot, C. Ernst, E. G. Fahnestock, M. Kueppers, P. Pravec, E. Rainey, D. C. Richardson, A. M. Stickle, and C. Thomas, "AIDA DART asteroid deflection test: Planetary defense and science objectives," *Planetary and Space Science*, Vol. 157, 2018, pp. 104–115.

[10] S. Naidu, L. Benner, M. Brozovic, M. Nolan, S. Ostro, J. Margot, J. Giorgini, T. Hirabayashi, D. Scheeres, P. Pravec, P. Scheirich, C. Magri, and J. Jao, "Radar observations and a physical model of binary near-Earth asteroid 65803 Didymos, target of the DART mission," *Icarus*, Vol. 348, 2020, p. 113777.

[11] R. T. Daly, C. M. Ernst, O. S. Barnouin, N. L. Chabot, A. S. Rivkin, A. F. Cheng, E. Y. Adams, H. F. Agrusa, E. D. Abel, A. L. Alford, *et al.*, "Successful kinetic impact into an asteroid for planetary defence," *Nature*, Vol. 616, No. 7957, 2023, pp. 443–447.
[12] D. Scheeres, S. Ostro, R. Hudson, and R. Werner, "Orbits Close to Asteroid 4769 Castalia," *Icarus*, Vol. 121, No. 1, 1996, pp. 67–87.
[13] J. Miller, A. Konopliv, P. Antreasian, J. Bordi, S. Chesley, C. Helfrich, W. Owen, T. Wang, B. Williams, D. Yeomans, and D. Scheeres, "Determination of Shape, Gravity, and Rotational State of Asteroid 433 Eros," *Icarus*, Vol. 155, No. 1, 2002, pp. 3–17.
[14] D. Scheeres, "Dynamics about Uniformly Rotating Triaxial Ellipsoids: Applications to Asteroids," *Icarus*, Vol. 110, No. 2, 1994, pp. 225–238.
[15] D. Scheeres, S. Ostro, R. Hudson, E. DeJong, and S. Suzuki, "Dynamics of Orbits Close to Asteroid 4179 Toutatis," *Icarus*, Vol. 132, No. 1, 1998, pp. 53–79.
[16] D. Scheeres, B. G. Williams, and J. K. Miller, "Evaluation of the dynamic environment of an asteroid: Applications to 433 Eros," *Journal of Guidance, Control, and Dynamics*, Vol. 23, No. 3, 2000, pp. 466–475.
[17] G. M. Brown and D. J. Scheeres, "Temporal evolution of the dynamical environment around asteroid (101955) Bennu," *Icarus*, Vol. 403, 2023, p. 115632.
[18] S. Kikuchi, Y. Mimasu, Y. Takei, T. Saiki, D. J. Scheeres, M. Hirabayashi, K. Wada, M. Yoshikawa, S. i. Watanabe, S. Tanaka, and Y. Tsuda, "Preliminary design of the Hayabusa2 extended mission to the fast-rotating asteroid 1998 KY26," *Acta Astronautica*, Vol. 211, 2023, pp. 295–315.
[19] G. M. Brown and D. J. Scheeres, "Analyzing the structure of periodic orbit families that exist around asteroid (101955) Bennu," *Celestial Mechanics and Dynamical Astronomy*, Vol. 135, No. 6, 2023, p. 52.
[20] D. J. Scheeres, "Orbit mechanics about asteroids and comets," *Journal of Guidance, Control, and Dynamics*, Vol. 35, No. 3, 2012, pp. 987–997.
[21] C. Buonagura, M. Pugliatti, and F. Topputo, "Image Processing Robustness Assessment of Small-Body Shapes," *The Journal of the Astronautical Sciences*, Vol. 69, No. 6, 2022, pp. 1744–1765.
[22] G. Bellei, J. L. Cano, and M. Sánchez, "Operational orbiting strategies about minor bodies," *21st International Symposium on Space Flight Dynamics ISSFD*, 2009.
[23] A. W. Harris and A. W. Harris, "On the Revision of Radiometric Albedos and Diameters of Asteroids," *Icarus*, Vol. 126, No. 2, 1997, pp. 450–454.
[24] B. Carry, "Density of asteroids," *Planetary and Space Science*, Vol. 73, No. 1, 2012, pp. 98–118.
[25] A. Fitzgibbon, M. Pilu, and R. Fisher, "Direct Least-Squares fitting of ellipses," *Pattern Analysis and Machine Intelligence, IEEE Transactions on*, Vol. 21, 1996, pp. 253–257.
[26] P. T. Wittick and R. P. Russell, "Mixed-model gravity representations for small celestial bodies using mascons and spherical harmonics," *Celestial Mechanics and Dynamical Astronomy*, Vol. 131, 2019, pp. 1–29.
[27] R. Russell and P. Wittick, "Mascon Models for Small Body Gravity Fields," 2017.
[28] T. Chanut, S. Aljbaae, and V. Carruba, "Mascon gravitation model using a shaped polyhedral source," *Monthly Notices of the Royal Astronomical Society*, Vol. 450, No. 4, 2015, pp. 3742–3749.
[29] V. A. Chobotov, *Orbital mechanics*. AIAA, 2002.
[30] Y. Takahashi, D. J. Scheeres, and R. A. Werner, "Surface gravity fields for asteroids and comets," *Journal of guidance, control, and dynamics*, Vol. 36, No. 2, 2013, pp. 362–374.